Supplementary material for: Shunt peaking in neural membranes

Francisco J. H. Heras, Simon B. Laughlin, Jeremy E. Niven

September 29, 2016

1 Supplementary methods

1.1 Blowfly photoreceptor membrane model

We modelled a blowfly (*Calliphora vicina*) R1-6 photoreceptor membrane (Figure 1a). The R1-6 photoreceptors of female blowflies are between 220 and 280 µm in length [1], with a membrane capacitance of $C = 0.13\,\mathrm{nF}$ [2]. These photoreceptors express two voltage-dependent K^+ conductances [2]: the fast delayed rectifier (FDR) and the slow delayed rectifier (SDR). The SDR activates more slowly than the FDR (5-40 ms vs 1-10 ms), and has 15 mV higher activation range [2]. Their activation ranges span the physiological voltage range of the photoreceptor. Although a very slow (>1 s) inactivation has been reported for both K^+ conductances, we model them as non-inactivating, mainly for simplicity and because the reported inactivation was partial (20-25%) [2].

The FDR was modelled using a Hodgkin-Huxley type model with a single activation variable [3]. The steady-state conductance of the FDR at a membrane voltage V, $g_{\mathrm{F},\infty}(V)$, fits the Boltzmann distribution:

$$g_{\mathrm{F},\infty}(V) = \bar{g}_{\mathrm{F}} \frac{1}{1 + \exp(-\frac{V - V_{\mathrm{shift}} + a}{b})} \tag{1}$$

where $a = 65$ mV and $b = 8.5$ mV [2], and $\bar{g}_{\mathrm{F}}$ is the maximum conductance. A voltage shift of $V_{\mathrm{shift}} = 15$ mV applied to the patch clamp results was deemed necessary to reproduce the *in vivo* behaviour of the conductance [2, 4].

The activation time constant of the FDR was as fitted by Gerster *et al.* [4] using patch clamp data from Weckström *et al.* [2] that had already been shifted by 15 mV:

$$\tau_{\mathrm{F}}(V) = \frac{1}{a \exp(V/b) + c \exp(V/d)} \tag{2}$$

where $a = 3\,\mathrm{ms}^{-1}$, $b = 24.4\,\mathrm{mV}$, $c = 9.4 \times 10^{-8}\,\mathrm{ms}^{-1}$ and $d = -7.8\,\mathrm{mV}$.

The SDR was similarly modelled using a Hodgkin-Huxley framework with a single activation variable [2]:

$$g_{\mathrm{S},\infty}(V) = \bar{g}_{\mathrm{S}} \frac{\alpha(V)}{\alpha(V) + \beta(V)} \tag{3}$$

$$\tau_{\mathrm{S}}(V) = \frac{1}{\alpha(V) + \beta(V)} \tag{4}$$

where the activation and deactivation functions are respectively $\alpha = 0.9\exp((V - V_{\mathrm{shift}})/13)$ and $\beta = 0.0037\exp(-(V - V_{\mathrm{shift}})/33.8)$.

The maximum conductance values, $\bar{g}_{\mathrm{F}} = \bar{g}_{\mathrm{S}} = 30$ nS for both conductances, were chosen to give an input resistance of $\sim$27 MΩ. This is intermediate among the values of 20 to 34 MΩ obtained in previous articles [2, 5, 6].

To reverse the ion flux, the photoreceptor membrane expresses Na^+/K^+ ATPases with very slow dynamics [7, 8, 4]. We assume that these molecular pumps reverse the outflux of K^+ ions flowing through the delayed rectifiers in the steady state, producing with a net hyperpolarising current [8].

Fly R1-6 photoreceptors also express a Na^+/Ca^{2+} exchanger that extrudes Ca^{2+} from the microvilli [9, 10, 11, 12, 13]. This Ca^{2+} current is small relative to the light-induced current (26% in *Drosophila* [13]), producing a net current much smaller than the pump current. Consequently, the Na^+/Ca^{2+} exchanger was not implemented in the model.

To prevent the dark-adapted photoreceptor membrane potential from dropping to the K^+ reversal potential, $E_{\mathrm{K}} = -85$ mV [2], we introduced a depolarising leak conductance into the model. If we assume that it has the same reversal potential as light-induced current, $E_{\mathrm{L}} = 5$ mV, the depolarising leak must have a conductance of $g_{\mathrm{leak}} = 5.4$ nS. In the light-adapted photoreceptor, a light conductance of $g_{\mathrm{light}} = 47.4$ nS was used to depolarise the photoreceptor to −40 mV.

1.2 Drone photoreceptor membrane model

We modelled the drone honeybee (*Apis melliphera*) photoreceptor membrane after Vallet *et al.* [14] (Figure 2a). The only outward current in this model is K^+. We consider the K^+ conductance, g_{K}, to be voltage-independent and to have a reversal potential of $E_{\mathrm{K}} = -66$ mV. Opposing this current, there is a light-induced current with a reversal potential of $E_{\mathrm{L}} = 0$ mV and a voltage-dependent Na^+ current with reversal potential of $E_{\mathrm{Na}} = 57$ mV.

The Hodgkin-Huxley model [3] for the Na^+ conductance in the squid giant

axon is:

$$I_{\mathrm{Na}} = \overline{g_{\mathrm{Na}}} m^3 h (E_{\mathrm{Na}} - V) \tag{5}$$

$$\alpha_m = \frac{0.1(-V + V_{\mathrm{r}} + 25)}{\exp[(-V + V_{\mathrm{r}} + 25)/10] - 1} \tag{6}$$

$$\beta_m = 4 \exp(-(V - V_{\mathrm{r}})/18) \tag{7}$$

$$\alpha_h = 0.07 \exp(-(V - V_{\mathrm{r}})/20) \tag{8}$$

$$\beta_h = \frac{1}{\exp(-V + V_{\mathrm{r}} + 30)/10) + 1} \tag{9}$$

Vallet *et al.* [14] found that multiplying both α_h and β_h by a factor $k_h = 0.1$, i.e. making the inactivation time constant 10 times slower, gave a better fit to the drone photoreceptor electrical responses. The dark adapted rest potential is taken to be $V_{\mathrm{r}} = -55.5\,\mathrm{mV}$ and the maximum Na^+ is $\overline{g_{\mathrm{Na}}} = 4\,\mathrm{mS\,cm^2}$.

Following Vallet *et al.* [14], we used a voltage-independent K^+ conductance $g_{\mathrm{K}} = 0.2\,\mathrm{mS\,cm^2}$. To depolarise the cell to a light-adapted membrane voltage of $V = -38\,\mathrm{mV}$, we introduced a total depolarising conductance with the reversal potential of light current of $g_{\mathrm{L}} = 0.11\,\mathrm{mS\,cm^2}$.

Vallet *et al.* [14] did not provide any absolute values for the drone photoreceptor size or membrane capacitance. To facilitate comparisons with the blowfly photoreceptor membrane we used the same membrane area, $1.3 \times 10^{-4}\,\mathrm{cm^2}$. This affects absolute values of impedance and currents but not the results presented in our article, which only depend upon the shape of the impedance function or the balance between currents, and are unaffected by scaling the photoreceptor while keeping constant the conductance densities.

1.3 Obtaining the steady-state currents

The steady-state values of the conductances at different membrane potentials were calculated using well-known procedures (e.g. [6]). Each light intensity generates a light-induced conductance, g_{light}, and the corresponding depolarisation a total K^+ conductance, g_{K}. The K^+ and light-induced currents flowing through the conductances are given by:

$$I_{\mathrm{K}} = (E_{\mathrm{K}} - V) g_{\mathrm{K}}(V) \tag{10a}$$

$$I_{\mathrm{L}} = (E_{\mathrm{L}} - V) g_{\mathrm{L}} \tag{10b}$$

where $g_{\mathrm{K}} = g_{\mathrm{K,F}}(V) + g_{\mathrm{K,S}}(V)$ is the total K^+ conductance and g_{L} is the total depolarising conductance, the sum of both the leak conductance and the light-induced conductance $g_{\mathrm{L}} = g_{\mathrm{light}} + g_{\mathrm{leak}}$.

The Na^+/K^+ ATPase maintains the ionic concentration in the photoreceptor by pumping 2 K^+ ions in and 3 Na^+ ions out in each cycle [7]. Assuming that the Na^+/K^+ ATPase maintains the internal K^+ concentration constant, this produces a net pump current, I_{P} of the same sign and half the size of the K^+ current [8, 15]:

$$I_{\mathrm{P}} = I_{\mathrm{K}}/2 \tag{11}$$

By combining Equations 10 and Equation 11 with the condition for zero net current across the membrane at the steady state:

$$I_{\mathrm{P}} + I_{\mathrm{K}} + I_{\mathrm{L}} = 0 \tag{12}$$

we obtain:

$$\frac{3}{2}(E_{\mathrm{K}} - V)g_{\mathrm{K}}(V) + (E_{\mathrm{L}} - V)g_L = 0 \tag{13}$$

To obtain the total depolarizing conductance, g_{L}, we solve Equation 13. We first solve it for the dark adapted photoreceptor to obtain g_{leak}, and then to the light-adapted photoreceptor to obtain $g_{\mathrm{light}} = g_{\mathrm{L}} - g_{\mathrm{leak}}$.

In the case of the drone membrane, the equivalent current equations are:

$$I_{\mathrm{K}} = (E_{\mathrm{K}} - V)g_{\mathrm{K}} \tag{14a}$$

$$I_{\mathrm{Na}} = (E_{\mathrm{Na}} - V)g_{\mathrm{Na}}(V) \tag{14b}$$

$$I_{\mathrm{L}} = (E_{\mathrm{L}} - V)g_{\mathrm{L}} \tag{14c}$$

where the only voltage-dependent conductance is the Na^+ conductance, $g_{\mathrm{Na}}(V)$.

To follow more closely the model fitted by Vallet *et al.* [14], neither the Na^+/K^+ ATPase nor the Na^+/Ca^{2+} exchanger were included in the drone bee photoreceptor membrane model. Hence, instead of Equation 13, we obtain:

$$(E_{\mathrm{K}} - V)g_{\mathrm{K}} + (E_{\mathrm{Na}} - V)g_{\mathrm{Na}}(V) + (E_{\mathrm{L}} - V)g_{\mathrm{L}} = 0 \tag{15}$$

This equation is the equivalent to Equation 13, and at each membrane voltage, V, it can be solved to obtain the needed depolarizing light conductance, g_{L}.

1.4 Current injection

To obtain the impedance, we drove the photoreceptor membrane model with Gaussian white noise (WN) current of zero mean, $I(t)$, around a steady-state voltage, V_0. This implies first obtaining the light conductance, g_{L}, and the pump current, $I_{\mathrm{P}}(V_0)$, corresponding to the membrane voltage V_0, as explained in the previous subsection. Then, we numerically solved the system of ordinary differential equations composed by the HH equations for the voltage-dependent conductance ($g_{\mathrm{K}}(V)$ for the blowfly and $g_{\mathrm{Na}}(V)$ for the drone photoreceptor) and the following equation:

$$\frac{dV}{dt} = \frac{1}{C}\left[I(t) + I_{\mathrm{P}}(V_0) + \sum I_{\mathrm{conductances}}(V)\right] \tag{16}$$

where the sum $\sum I_{\mathrm{conductances}}(V)$ runs over the conductances in the respective membranes (Equation 10 for the blowfly and Equation 14 for the drone photoreceptor). Note that during each simulation we treat the pump as a fixed current, $I_{\mathrm{P}}(V_0)$, with its steady-state value calculated as in Equation 11 in the case of the blowfly and $I_{\mathrm{P}}(V_0) = 0$ in the case of the drone photoreceptor. This is reasonable due to its slow dynamics and the small voltage deflections that we consider.

The steady-state voltage, V_0, was either rest ($-60\,\mathrm{mV}$ in the blowfly, $-55.5\,\mathrm{mV}$ in the drone), or a depolarized light-adapted voltage ($-40\,\mathrm{mV}$ in the blowfly, $-38\,\mathrm{mV}$ in the drone). The WN was generated using the Mersenne Twister algorithm (NumPy version 1.8.2) and filtered using a 6^{th}-order Butterworth filter at $1000\,\mathrm{Hz}$ (SciPy version 0.13.3). Sampling was the same as the fixed time step of integration, $0.05\,\mathrm{ms}$, thus oversampling 10 times. A forward Euler integrator with fixed time step of integration was used to integrate the differential equations.

We used a WN sample of $10\,\mathrm{s}$ of duration, and then divided both current stimulus and voltage response in ten $1\,\mathrm{s}$ intervals. To numerically calculate the impedance $Z(f)$, we divide the cross-power spectral densities (CPSD) of the stimulus and the response by the stimulus power spectral density (PSD) [16, 17]:

$$Z(f) = \frac{\mathrm{CPSD}(f)}{\mathrm{PSD}(f)} = \frac{\langle V(f) I^*(f) \rangle}{\langle I(f) I^*(f) \rangle} \tag{17}$$

where $\langle\rangle$ denotes averages across the 10 time bins and the asterisk represents complex conjugation. $V(f)$ and $I(f)$ are the Fourier transforms of voltage response and current stimulus respectively, previously windowed by a Hamming function.

The impedance at each frequency is a complex number with a modulus, $|Z(f)|$, the impedance gain, and an argument, $\phi(f) = \arg[Z(f)]$, called the phase shift [17, 18, 19]. As it is usual practice (e.g. [20, 21]) we will call phase lag to the phase shift with a change of sign, and we will avoid the term phase delay which can have different meanings.

1.5 A closed formula for the membrane impedance

The response of a voltage-dependent conductance to small perturbations around a given voltage, V_0, is the same as the response of an electrical circuit with passive elements [22, 23, 24]. In the case of a non-inactivating voltage-dependent K^+ conductance, $g = \bar{g} n^\gamma$, the equivalent circuit is composed by a resistance R in parallel with a branch of a resistance r and an inductance L in series. Their numerical values are given by:

$$R = \frac{1}{\bar{g}\; n_\infty^\gamma} \tag{18a}$$

$$r = \frac{\alpha + \beta}{\gamma\; \bar{g}\; n^{\gamma-1}(V - E_{\mathrm{K}})[\alpha' - n(\alpha' + \beta')]} = \frac{1}{(V - E_{\mathrm{K}})\frac{\mathrm{d}}{\mathrm{d}V}\,(1/R)} \tag{18b}$$

$$L = \frac{r}{\alpha + \beta} = \tau r \tag{18c}$$

where $\alpha = \alpha(V)$, $\beta = \beta(V)$, $\tau = \tau(V)$ are respectively the activation rate, deactivation rate and time constant of the HH variable m at the voltage V, E_{K} is the reversal potential and a prime (') represents the derivative with respect to voltage.

In the blowfly photoreceptor, we are dealing with a simpler case where the conductance has only one gated particle, $\bar{g}n$. The simplified expressions are:

$$R = \frac{1}{\bar{g}\ n_\infty(V)} \tag{19a}$$

$$r = \frac{1}{(V - E_{\mathrm{K}})\frac{\mathrm{d}}{\mathrm{d}V}\,(1/R)} \tag{19b}$$

$$L = \frac{r}{\alpha + \beta} = \tau r \tag{19c}$$

We then use R, r and L to compute the impedance of the K^+ voltage-dependent conductance:

$$Z_{\mathrm{c}}^{-1}(f) = \frac{1}{R} + \frac{1}{r + i2\pi f L} = \frac{1}{R} + \frac{1/r}{1 + i2\pi f \tau} \tag{20}$$

The electrical circuit approximating the behaviour of the photoreceptor membrane is that formed by the light-gated and leak conductances, the RrL equivalent circuit of the two delayed rectifiers and the membrane capacitance, C. The resulting impedance is:

$$Z(f) = \frac{1}{Z_{\mathrm{F}}^{-1}(f) + Z_{\mathrm{S}}^{-1}(f) + g_{K,\mathrm{leak}} + g_{\mathrm{light}} + g_{\mathrm{leak}} + Z_{\mathrm{C}}^{-1}(f)} \tag{21}$$

where $Z_{\mathrm{F}}(f)$ and $Z_{\mathrm{S}}(f)$ are the impedances of the fast and slow rectifiers respectively (Equation 20), and $Z_C(f) = 1/i2\pi fC$ is the impedance of the membrane capacitance.

Similarly, the impedance of the Na^+ conductance, Z_{Na} is calculated using its equivalent RrL circuit. Its conductance has the form $g = \bar{g}m^\gamma h$, and then the electrical elements of the RrL equivalent circuit have the values:

$$R = \frac{1}{\bar{g}\ m^\gamma h} \tag{22a}$$

$$r = \frac{\alpha + \beta}{\gamma\ \bar{g}\ m^{\gamma-1}h(V - E_{\mathrm{K}})[\alpha' - m(\alpha' + \beta')]} = \frac{1}{(V - E_{\mathrm{K}})\bar{g}h\frac{\mathrm{d}}{\mathrm{d}V}m^\gamma} \tag{22b}$$

$$L = \frac{r}{\alpha + \beta} = \tau r \tag{22c}$$

$$r_h = \frac{\alpha_h + \beta_h}{\bar{g}\ m^\gamma(V - E_{\mathrm{K}})[\alpha'_h - h(\alpha'_h + \beta'_h)]} = \frac{1}{(V - E_{\mathrm{K}})\bar{g}m^\gamma\frac{\mathrm{d}}{\mathrm{d}V}h} \tag{22d}$$

$$L_h = \frac{r_h}{\alpha_h + \beta_h} = \tau_h r_h \tag{22e}$$

where $\alpha_h = \alpha_h(V)$, $\beta_h = \beta_h(V)$, $\tau_h = \tau_h(V)$ are respectively the activation rate, deactivation rate and time constant of the conductance of the HH inactivation variable h at the voltage V.

The electrical circuit approximating the behaviour of the whole photoreceptor membrane is that formed by the light-gated conductance, the voltage-independent K^+ conductance, the RrL equivalent circuit of the Na^+ conductance, and the membrane capacitance, C. The resulting impedance is:

$$Z(f) = \frac{1}{Z_{\mathrm{Na}}^{-1}(f) + g_{\mathrm{K}} + g_{\mathrm{L}} + Z_{\mathrm{C}}^{-1}(f)} \tag{23}$$

where $Z_C(f) = 1/i2\pi fC$ is the impedance of the membrane capacitance.

In both of the cases above, the effect of freezing the channel —i.e. to keep the gating variables constant while studying small perturbations around the steady state— is captured by removing the phenomenological branches. As expected, a frozen conductance has impedance equal to its resistance. When only one gating variable is frozen, the corresponding phenomenological branch disappears.

1.6 Q value

The band-pass of a membrane can be characterized by the Q value, the ratio of the maximum impedance gain to the input resistance [24, 25]. Under this definition, a low pass membrane has a Q value of 1 and the sharper the peak of a band-passing membrane, the higher the Q value. This Q value is different from the Q factor, widely used in engineering to quantify resonances.

1.7 GBWP

For the purposes of defining the gain bandwidth product (GBWP), we used the following definition: gain is the maximum impedance gain, while bandwidth is the value of the frequency where the impedance gain drops below $1/\sqrt{2}$ the maximum value, approximately the -3 dB upper cut-off frequency [26, Section 12.3].

1.8 Group delay

The group delay $t_g(f)$ is obtained as a derivative of the phase lag:

$$t_g(f) = -\frac{1}{2\pi}\frac{\mathrm{d}\phi(f)}{\mathrm{d}f} \tag{24}$$

It is a measure of the time delay between current injection and voltage response. If different frequencies arrive with different delays, the signal is distorted. Therefore, it is preferably to have a group delay as constant as possible in a particular range of frequencies.

We define group delay dispersion (GDD), as the standard deviation of group delay across a range of frequencies:

$$GDD = \sqrt{\frac{1}{f_2 - f_1}\int_{f_1}^{f_2} (t_g(f) - \overline{t_g})^2 df} \tag{25}$$

where $\overline{t_g}$ is the average group dispersion in the same range of frequencies.

1.9 Stability and minimum phase

Each of the equivalent circuits of the model membranes considered here contains two phenomenological branches. In the blowfly, they represent the activation of the FDR and SDR, while in the drone, they represent the activation and inactivation of the Na^+ conductance. As we will be treating both membranes at the same time, we can call the elements of these branches r_1, L_1, r_2 and L_2. The impedance of the photoreceptor for small signals around a particular membrane voltage V_0, Equations 21 and 23, can be written as:

$$Z(s) = \frac{R}{1 + st + \frac{g_1}{1+\tau_1 s} + \frac{g_2}{1+\tau_2 s}} = \frac{R(1+s\tau_1)(1+s\tau_2)}{(1+st)(1+s\tau_1)(1+s\tau_2) + g_1(1+s\tau_2) + g_2(1+s\tau_1)} \tag{26}$$

where now we adopted the Laplace notation with complex number frequency s. R is the membrane resistance, $t = RC$ is the passive time constant of the membrane, $\tau_i = \frac{L_i}{r_i}$ the time constant of each branch and $g_i = R/r_i$ the conductance of each branch as a fraction of the membrane conductance.

The poles of Equation 26 are the zeroes of the denominator, which is a third degree polynomial:

$$(1 + g_1 + g_2) + s(t + \tau_1 + \tau_2 + g_1\tau_2 + g_2\tau_1) + s^2(\tau_1\tau_2 + t\tau_1 + \tau_2 t) + s^3 t\tau_1\tau_2 \tag{27}$$

When all coefficients in the polynomial are positive and the following inequality holds:

$$(t + \tau_1 + \tau_2 + g_2\tau_1 + g_1\tau_2)(\tau_1\tau_2 + t\tau_2 + \tau_1 t) > t\tau_1\tau_2(1 + g_2 + g_1) \tag{28}$$

the Routh-Hurwitz criterion says that all the zeroes of the Polynomial 27, and thus all the poles of Equation 26, have a negative real part. This is true always in the blowfly photoreceptor membrane model (as both $g_1, g_2 > 0$), but depending on the values it can be false in the drone photoreceptor model.

The zeros of Equation 26 are $s = \{-1/\tau_1, -1/\tau_2\}$, which are both negative real numbers.

If both the poles and zeroes of the transfer function in Equation 26 have a negative real part, the linearised membrane is stable and minimum phase [27]. Stability here means that any bounded input produces a bounded output, and in particular that the voltage does not vary if there is no current input. Minimum phase means that group delay is minimum among all the transfer functions with the same gain.

2 Supplementary results

2.1 Simulated voltage responses to current pulses in the time domain agree with experimental results and illustrate the linear behaviour of the membrane

The photoreceptor membrane's voltage response to injected current pulses is asymmetric (Figure S1a). This well known behaviour is due to the change in conductance with time and voltage of the two delayed rectifier conductances [2]. Without them, the membrane behaves as a passive RC circuit, which is linear and thus symmetrical to positive and negative pulses. Both the asymmetric response to positive and negative pulses and the size of the voltage deflections compare well with experimental results, thereby validating the model (Figure S1b).

The voltage response to the injection of smaller current pulses (0.05 nA) becomes symmetrical, with responses of the same magnitude to negative and positive current pulses (Figure S2a). This is an indication (but not a proof) that the system may be approaching its linear regime, as linearity implies symmetry to negative and positive pulses. To see that indeed the system behaves linearly, we can compare the responses of the simulation of the blowfly photoreceptor using Hodgkin and Huxley type equations with the responses of the linearisation —the RrLC equivalent circuit. For smaller current pulses they agree completely (dashed lines, Figure S2a). At high light levels, when membrane resistance is low, the linearisation gives a good prediction of the voltage response for current pulses of up to 0.7 nA (Figure S2b).

2.2 Changes in time constants affect the shape of voltage responses to injected current pulses in both the blowfly and the drone photoreceptor membrane

The voltage response to injected current pulse and impedance function change when the biophysical properties of the membrane conductances change, and in particular when the time constants change. In the main text we have illustrated this in the frequency domain, but it is instructive to analyse also the voltage responses in the time domain obtained with the HH simulation.

In the dark adapted R1-6 blowfly membrane, making the FDR activation time constant, τ_F, faster decreases the overshoot of the voltage response to 0.1 nA current pulses injection (Figure S3a) and decreases the membrane bandwidth (Figure S3b). Making the FDR activation slower increases the overshoot of the voltage response, which start to show underdamped oscillations (Figure S3a), and increases the band-passing behaviour of the membrane (Figure S3b).

In the light-adapted drone bee photoreceptor membrane we found a prominent peak in the impedance, a resonance (Figure 2b in the main text). In the time domain, we confirm the presence of both amplification and underdamped oscillations when injecting current in the light-adapted photoreceptor model

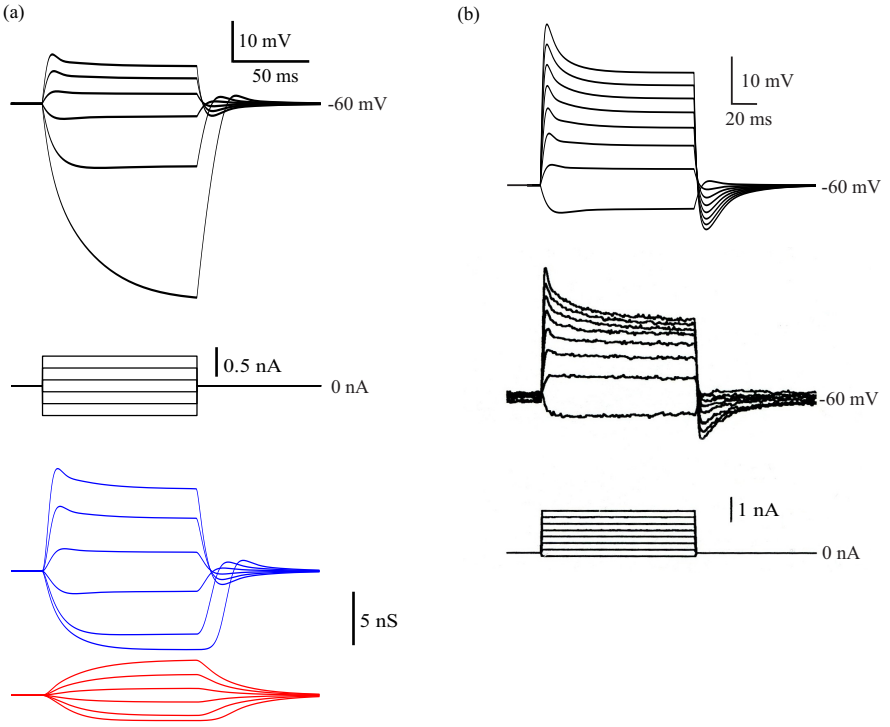

Figure S1: A Hodgkin-Huxley (HH) model reproduces the voltage responses of *C. vicina* R1-6 photoreceptors to injected current pulses. (a) (*Upper panel*) Voltage responses of the model photoreceptor to current pulses from resting potential ($-60\,\mathrm{mV}$). (*Middle panel*). The current pulses injected to produce the voltage responses. (*Lower panel*). Changes in the conductance of the fast (blue) and slow (red) delayed rectifiers evoked by the current pulses. (b) Comparison of the voltage responses of the photoreceptor model with those of a *C. vicina* photoreceptor recorded *in vivo*. (*Upper panel*). The voltage responses of the model *C. vicina* R1-6 photoreceptor to injected current. (*Middle panel*). The voltage responses of a *C. vicina* R1-6 photoreceptor recorded *C. vicina* to the same set of injected current pulses. Data reproduced from Anderson [28]. (*Lower panel*). The current pulses injected to produce the voltage responses.

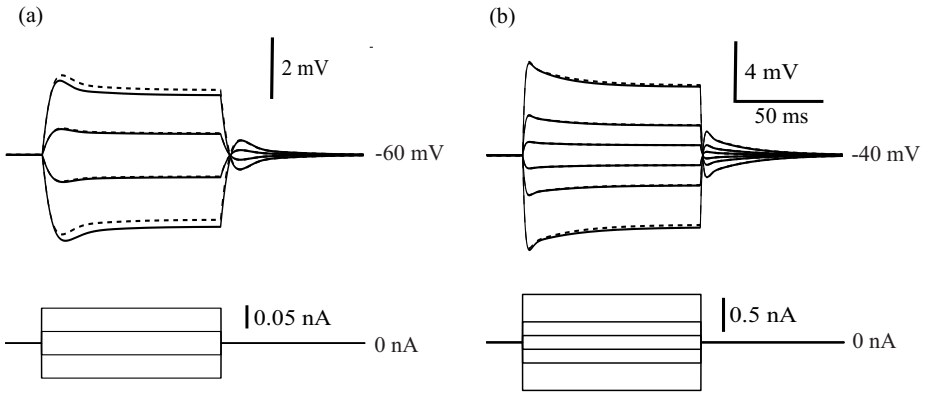

Figure S2: Small voltage responses of *C. vicina* photoreceptors differ from RC charging curves. (a) (*Upper panel*). Voltage responses evoked by small injected current pulses into the active photoreceptor membrane (black, solid) or the RrLC circuit (black, dashed) at rest. (*Lower panel*). The set of current pulses that evoked the voltage responses. (b) (*Upper panel*). At high light intensities that depolarise the photoreceptor to -40 mV, injected current pulses evoke small voltage responses from the active photoreceptor membrane containing voltage-dependent K^+ conductances (black, solid) and from a RrLC circuit (black, dashed). (*Lower panel*). The set of current pulses that evoked the voltage responses.

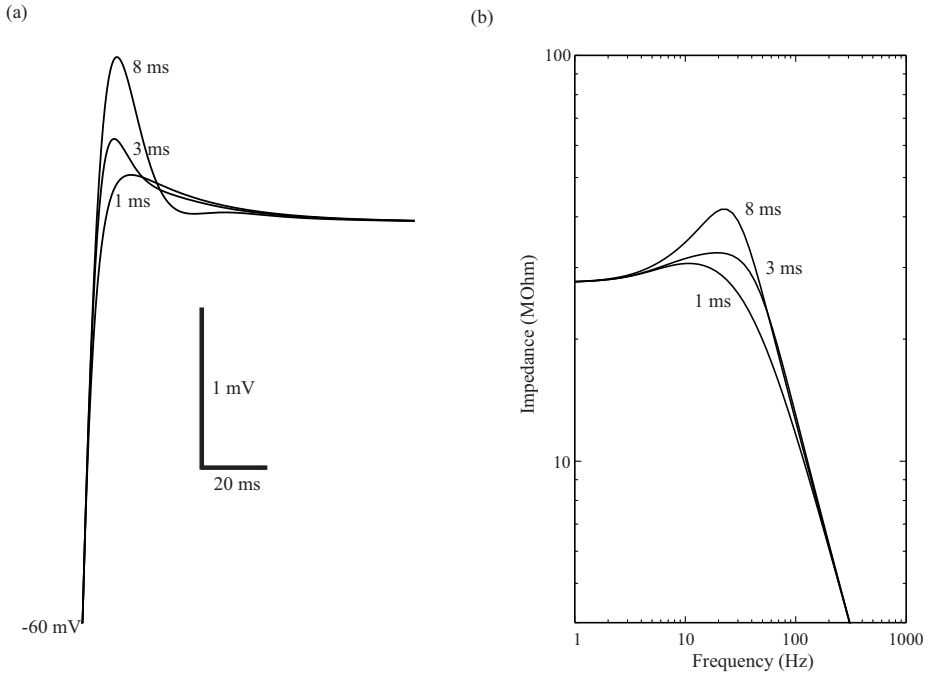

Figure S3: The voltage response to injected current changes with conductance activation time constants in the dark adapted blowfly R1-6 photoreceptor. (a) Voltage response to 0.1 nA current injections for three different FDR activation time constants. (b) Membrane impedance for three different FDR activation time constants.

(Figure S4a). Larger current injections produce spikes in the full HH simulation (not shown). The voltage responses of the HH model to smaller currents fit the linear model (Figure S4a, dashed lines).

The resonance disappears when τ_h, the time constant of Na^+ conductance inactivation, is made 10 times faster (Figure 2b in the main text). In the time domain, the voltage responses to injected current become smaller and the underdamped oscillations disappear (Figure S4b). The photoreceptor membrane also becomes more linear, as illustrated by comparing the voltage responses to the voltage responses of the equivalent RrLC circuit.

2.3 The fast delayed rectifier alone produces most of the shunt-peaking in the blowfly membrane

For both the dark and light-adapted photoreceptor, we modified the model to test for the impact of the FDR time constant, and the lack of SDR, on the GBWP. In a simplified membrane containing only a FDR conductance, when the SDR has been substituted with a voltage-independent conductance of the same value, changing the activation time constant, τ, of the FDR changes the shape of the filter from low pass to band pass. The frozen-SDR membrane with vanishingly small FDR activation time constant approaches the behaviour of the passive membrane, which is an RC low-pass filter, and thus its relative GBWP decreases towards 1 (Figure S5). The frozen-SDR membrane with short time constant of activation has a greater GBWP than the passive membrane, and it is still low-passing. For longer values of the activation time constant, $\tau > 2.81\,\text{ms}$, it becomes band-passing. If τ becomes even longer, the filtering is more and more restricted to low frequencies.

The relative GBWP of the dark adapted membrane initially improves as the activation time constant increases up to a broad maximum at 4 to 5 ms (Figure S5a). Further increases in the time constant produce slow decreases in GBWP. The maximum improvement in GBWP is 49% (i.e. relative GBWP of 1.49). For the optimum time constant, the membrane is band-passing ($Q > 1$). If we restrict ourselves to low-passing membranes, an activation time constant of $\tau = 2.81\,\text{ms}$ still boosts the GBWP by 46% (i.e. relative GBWP of 1.46). Thus, significant improvements of GBWP can be achieved by the use of delayed rectifiers while keeping low-pass filtering. Similarly, in the light-adapted membrane (Figure S5) there is a local maximum in relative GBWP of 1.26, that is obtained for an activation constant of 1.3 ms. In both cases, significant improvements of the GBWP in the blowfly membrane can be achieved by the use of the FDR.

The SDR slightly increases the GBWP in comparison with the model with only the FDR, both in the dark adapted and in the light-adapted membrane and with any choice of FDR activation time constant (dashed lines in Figure S5).

Thus, the delayed rectifiers in the blowfly membrane –particularly the FDR, with a time constant appropriate for shunt-peaking– increase the GBWP.

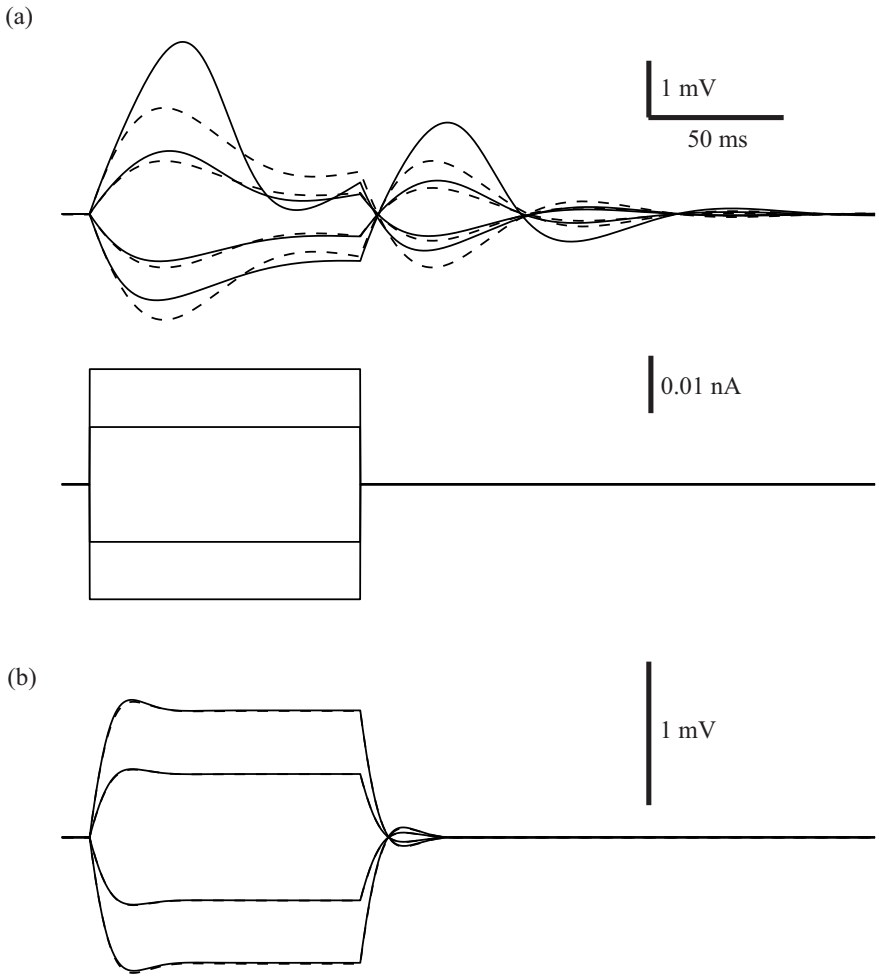

Figure S4: Voltage deflection of the light-adapted drone photoreceptor membrane (solid line) and the linearised membrane (dashed line) in response to small current injections of 100 ms (a) *(Upper panel)* If the Na^+ conductance has the dynamics used by Vallet *et al.* [14], voltage deflections of the drone membrane show underdamped oscillations. *(Lower panel)* Injected current pulses used to produce the voltage deflections. (b) If the dynamics of inactivation are accelerated 10-fold, oscillations are largely suppressed. If the same current pulses are injected, the voltage response is reduced by half.

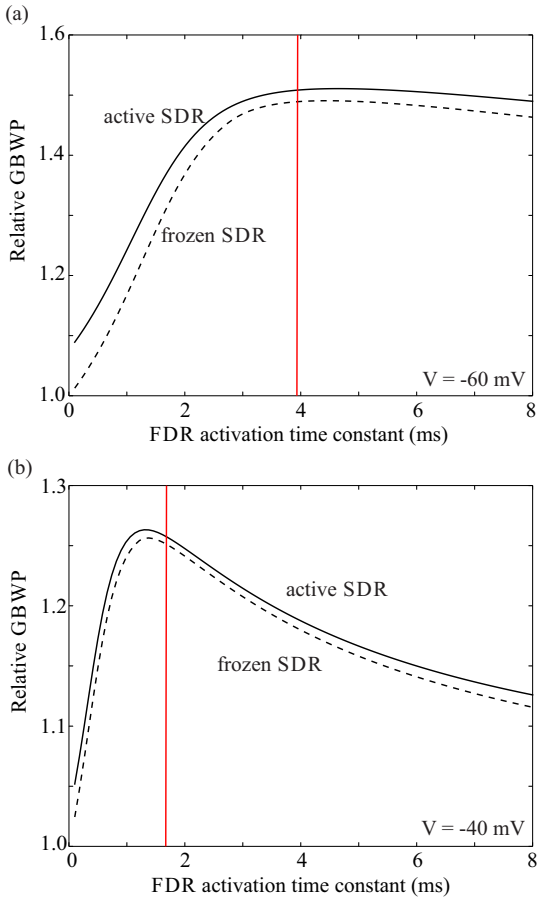

Figure S5: The fast delayed rectifier (FDR) in the blowfly photoreceptor improves the relative GBWP of its membrane. Relative GBWP as a function of FDR activation time constant. Solid lines are obtained with a voltage-dependent SDR and dashed lines by freezing the SDR at the steady state, i.e. by substituting the SDR by a voltage-independent K^+ conductance during the impedance calculation. Calculated both for dark adapted (a) and light-adapted (b) model photoreceptor membranes. In both cases, the FDR activation time constant that maximises GBWP is not far from the FDR activation time constant in the original model [2] (red vertical lines).

2.4 Effects of shunt-peaking on stability and phase

We have seen that the delayed rectifiers in the blowfly membrane and in the modified drone photoreceptor membrane produce shunt-peaking. Using the equations in Section 1.9, it can be seen that this increase in GBWP is achieved, at least in the linear domain, without renouncing to two important properties of the passive RC membrane. One is stability —bounded inputs produce bounded outputs— and the other is minimum-phase —any other membrane with the same gain function would have to have longer phase lags.

2.5 Effects of shunt-peaking on group delay distortion of the blowfly membrane

Arguably, the relevant measure for delay in the frequency domain is not the phase lag but the group delay [29, 30]. This is because the phase lag describes the delay between two infinitely long sinusoids (stimulus and response), while the group delay describes how much a change in envelope in a sinusoid is delayed between response and stimulus. The group delay is calculated as the first derivative of the phase lag respect to the angular frequency (Equation 24). Group delay is a function of frequency (Figure S6). Group delay of a passive RC membrane is positive at low frequencies and approaches zero at high frequencies (dashed lines, Figure S6). In the membrane with both FDR and SDR active, group delay at low frequencies becomes negative, then positive and finally it drops to zero at high frequencies (solid line). While passive membranes present always a positive group delay, active membranes can present negative group delay at low frequencies, when inductive effects dominate. This effect is more important in the light-adapted membrane, because of the more important activation of the SDR.

In general, group delay changes with frequency. This indicates that high and low frequencies are transmitted with different delays, producing a group delay dispersion (GDD). In addition to increase bandwidth, i.e. to have a reasonable gain across a large band of frequencies, the photoreceptor membrane should make the voltage signals arrive with similar delays, i.e. minimise the GDD. Inductive elements, in principle, can help to reduce the GDD [31].

GDD is usually quantified as the first derivative of group delay with respect to angular frequency. However, as here we are interested in the dispersion across many frequencies, we will quantify GDD in a different way, as the standard deviation of group delay in a band of frequencies, for example between 1 and 100 Hz (Equation 25). In a dark adapted photoreceptor, group delay dispersion can be reduced to 1.2 ms with a FDR activation time constant of 2 ms (Figure S7a). This is half the group delay dispersion of a passive membrane. In a light-adapted photoreceptor membrane, however, the group delay dispersion increases at least fourfold by the use of voltage-dependent conductances. We can see that this is due to the SDR, because if it is substituted by a voltage-independent conductance, group delay dispersion can be reduced, and almost suppressed with a FDR activation constant of 1 ms.

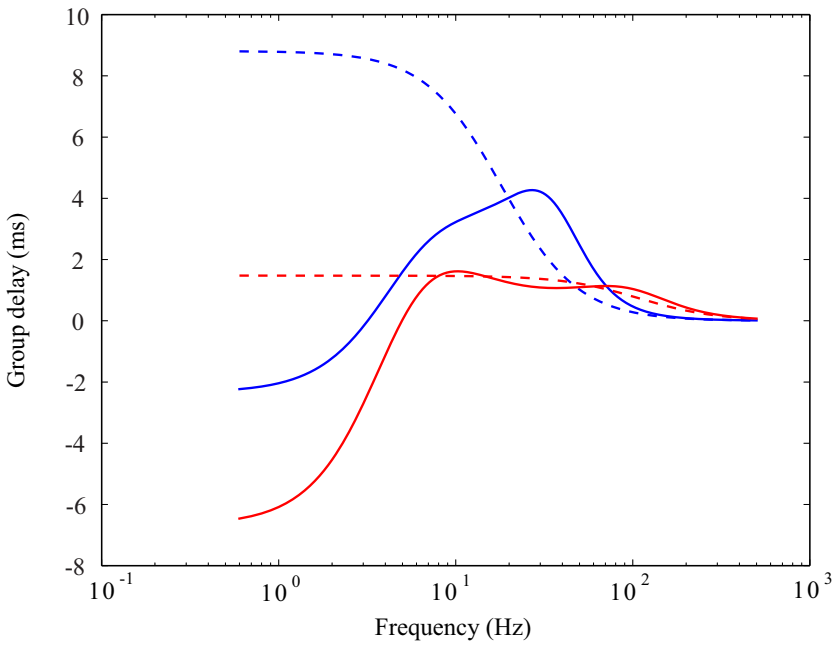

Figure S6: The delayed rectifiers modify the group delay. Group delay of active membranes (solid lines) compared to the group delay of passive membranes with the same membrane resistance and capacitance (dashed lines). The blue line corresponds to the dark adapted photoreceptor (-60 mV) and the red line to the light-adapted photoreceptor (-40 mV).

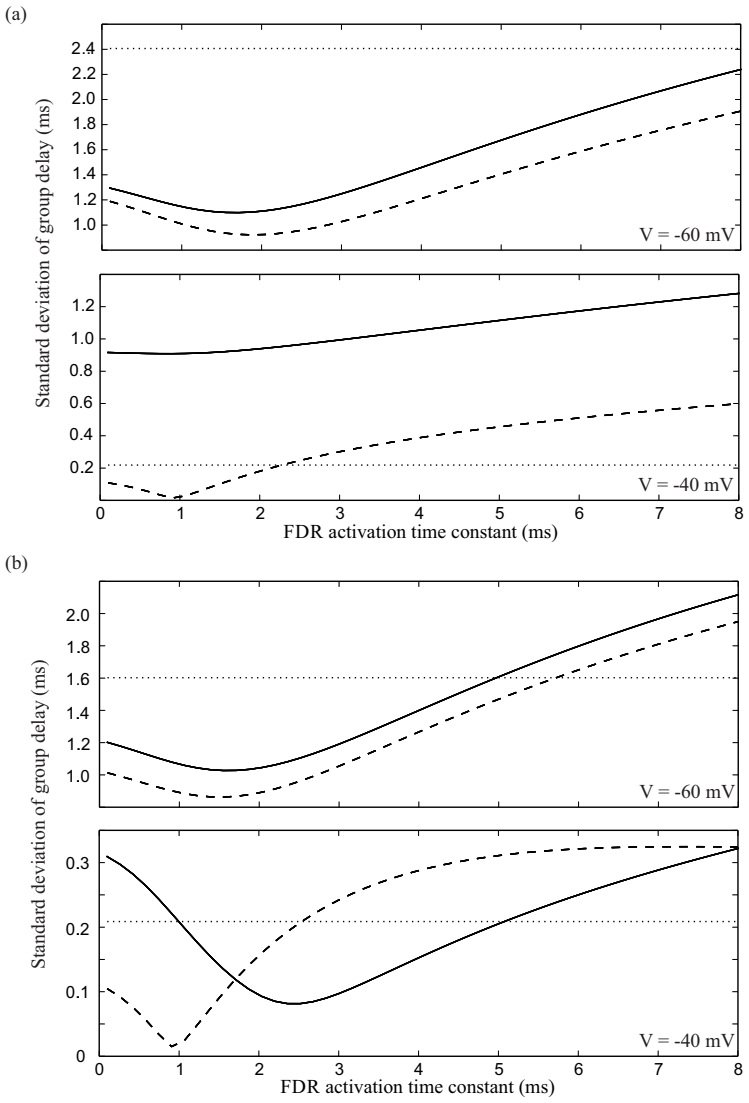

Figure S7: Standard deviation of group delay of blowfly R1-6 photoreceptor membranes changes with FDR activation time constant. Solid line is the full membrane model and dashed line is the model with voltage-independent SDR, both as a function of the FDR activation time constant. The standard deviation of group delay in a passive membrane with both FDR and SDR voltage-independent is shown in dotted line as a reference. (a) When the standard deviation of the group delay is calculated between 1 Hz and 100 Hz, either in a dark adapted photoreceptor membrane *(upper panel)* or in the membrane of photoreceptor depolarised by light to -40 mV *(lower panel)* (b) Same as (a) but when the standard deviation of the group delay is calculated between 10 Hz and 100 Hz.

This deleterious effect of the SDR on distortion is restricted to low frequencies, as we can see if we repeat the calculations above, but now restricting the frequency range to between 10 and 100 Hz. The effect of SDR in the dark adapted membrane is smaller, due to the very limited activation of SDR at $-60\,\mathrm{mV}$ (Figure S7b). In the light-adapted photoreceptor, the group delay dispersion can be now reduced below that of the passive membrane if the FDR activation time constant is between 1 ms and 5 ms. The effect of the SDR shifts the optimum FDR activation to longer time constants.

3 Supplementary discussion

3.1 Limitations

Our model of the photoreceptor omitted the axon. However, its high input resistance [33] means it would have a negligible effect on voltage responses in the cell body, except at the lowest light levels when coupling between photoreceptor axons can be important [34]. The relationship between current injection in the cell body and voltage response at the terminal are limited by the axon only at frequencies well above the membrane bandwidth [33]. If the axon is passive with reasonable assumptions about terminal resistance and membrane resistivity, the contribution of this short axon ($60\,\mu\mathrm{m}$) to group delay is of $0.1\,\mathrm{ms}$, and flat up to $100\,\mathrm{Hz}$ [33]. Hence, group delay dispersion of the membrane would coincide with the group delay dispersion between current injected in the cell body and voltage signal in the terminal.

3.2 Sensitivity to parameters

The shunt-peaking capabilities of a delayed rectifier depend on the time constant of activation. However, we can see (Figure 3,4d) how there is a wide range of choices of time constants where an important improvement of GBWP takes place. The finding that two completely different voltage-dependent conductances, the FDR and the inactivating Na^+ conductance, can also produce shunt peaking reinforces the robustness of the results.

The shunt peaking capabilities of the delayed rectifier decrease if the leakiness of the membrane is increased. However, this decrease happens in a continuous way. We can decrease the membrane resistance while keeping the membrane voltage constant by adding the right combination of voltage-independent K^+ and light-induced conductances. This produces a decrease in the maximum relative GBWP (Figure S8A). It also increases the activation time constant that maximises such GBWP (Figure S8B).

3.3 Main results hold even if light-induced conductance does not contribute to impedance

The light-gated channels that together produce the light-induced conductance are embedded in the microvillar membrane. Each microvillus is a long and slen-

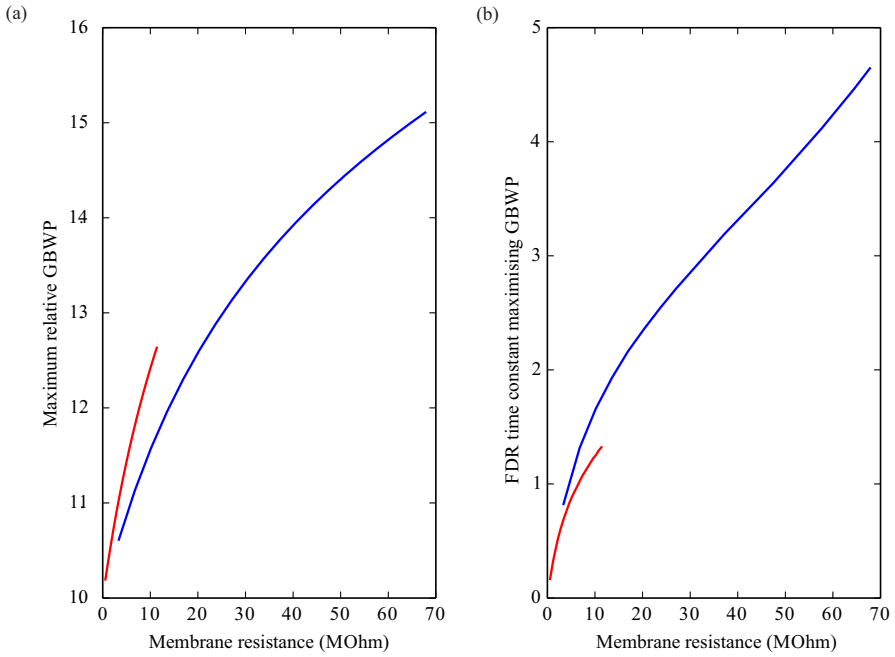

Figure S8: Decreasing the membrane resistance by the addition of voltage-independent conductances reduces the improvement in GBWP. (a) Maximum GBWP vs membrane resistance. GBWP is given as relative to the GBWP of a passive photoreceptor. (b) Activation time constant that maximizes GBWP as a function of membrane resistance. Blue line is the dark adapted photoreceptor and the red line is photoreceptor light-adapted to $-40\,\mathrm{mV}$.

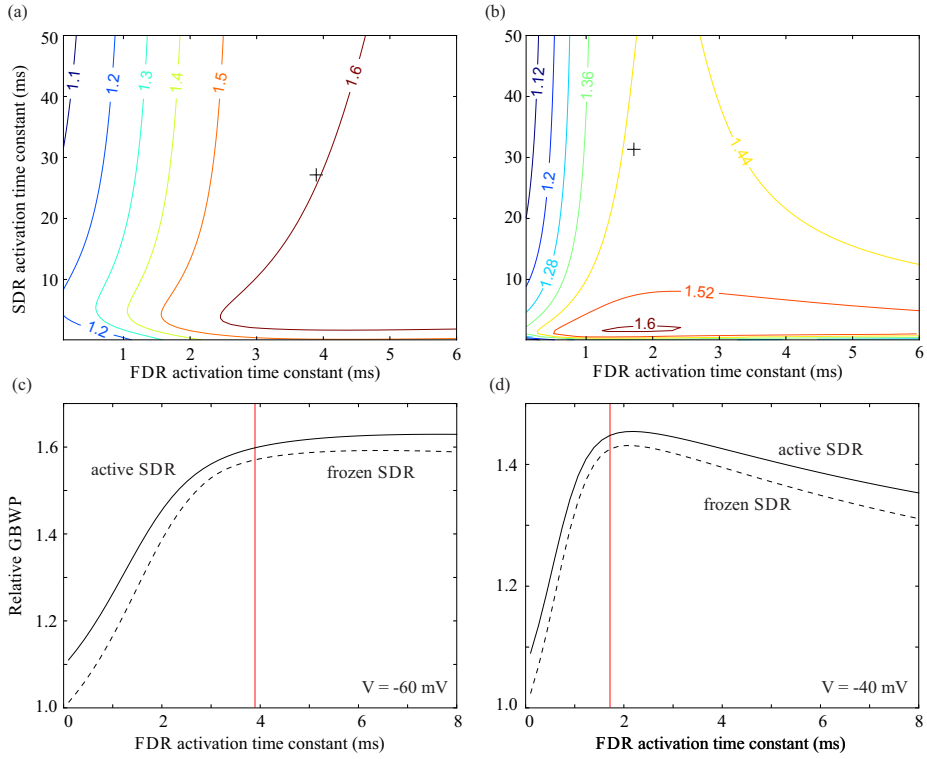

Figure S9: If the light-induced conductance does not contribute to impedance, FDR still produces shunt peaking. a) Same as Figure 1e, but with light-induced conductance not contributing to impedance. b) Same as Figure 1f. c) Same as Figure S5a. d) Same as Figure S5b.

der structure, connected to the photoreceptor cell body through a narrow neck, which it has been suggested to electrically isolate the microvilli from voltage changes in the cell body [32]. As a result, the light-induced conductance may be contributing less to the impedance than expected from its magnitude, and the effect of a change in light level would be more akin to a change in light-induced current than a change in conductance.

To show that our results hold even if that hypothesis is true, we modelled the most extreme case, i.e. the light-induced conductance and the leak conductance not contributing at all to the impedance. In that extreme case, shunt-peaking by the DRs is even more important than in the case where the light-induced conductance fully contributes to the impedance, improving the GBPW of the photoreceptor around 60% in the dark and 45% in moderate light levels (Figure S9 a, b, c, d).

The FDR is still the main contributor to shunt peaking, as it can be proved

by substituting the SDR by a voltage-independent conductance (Figure S9 c, d). Its time constant is still close to the one optimising shunt-peaking, both in the dark and light-adapted state.

References

[1] Hardie, R. C., 1985. Functional organization of the fly retina. In *Progress in Sensory Physiology* (eds. H. Autrum, D. Ottoson, E. R. Perl, R. F. Schmidt, H. Shimazu & W. D. Willis), volume 5 of *Progress in Sensory Physiology*, pp. 1–79. Springer Berlin Heidelberg.

[2] Weckström, M., Hardie, R. C. & Laughlin, S. B., 1991. Voltage-activated potassium channels in blowfly photoreceptors and their role in light adaptation. *J. Physiol.* **440**, 635–657.

[3] Hodgkin, A. L. & Huxley, A. F., 1952. A quantitative description of membrane current and its application to conduction and excitation in nerve. *J. Physiol.* **117**, 500–544.

[4] Gerster, U., Stavenga, D. G. & Backhaus, W., 1997. Na^+/K^+-pump activity in photoreceptors of the blowfly *Calliphora*: a model analysis based on membrane potential measurements. *J. Comp. Physiol. A* **180**, 113–122.

[5] Burton, B. G., Tatler, B. W. & Laughlin, S. B., 2001. Variations in photoreceptor response dynamics across the fly retina. *J. Neurophysiol.* **86**, 950–960.

[6] Niven, J. E., Anderson, J. C. & Laughlin, S. B., 2007. Fly photoreceptors demonstrate energy-information trade-offs in neural coding. *PLoS. Biol.* **5**, e116.

[7] Skou, J. C., 1957. The influence of some cations on an adenosine triphosphatase from peripheral nerves. *Biochim. Biophys. Acta* **23**, 394–401.

[8] Jansonius, N. M., 1990. Properties of the sodium pump in the blowfly photoreceptor cell. *J. Comp. Physiol. A* **167**, 461–467.

[9] Minke, B. & Armon, E., 1984. Activation of electrogenic Na-Ca exchange by light in fly photoreceptors. *Vis. Res.* **24**, 109–115.

[10] Hryshko, L. V., Matsuoka, S., Nicoll, D. A., Weiss, J. N., Schwarz, E. M., Benzer, S. & Philipson, K. D., 1996. Anomalous regulation of the *Drosophila* Na^+-Ca^{2+} exchanger by Ca^{2+}. *J. Gen. Physiol* **108**, 67–74.

[11] Wang, T., Xu, H., Oberwinkler, J., Gu, Y., Hardie, R. C. & Montell, C., 2005. Light activation, adaptation, and cell survival functions of the Na^+/Ca^{2+} exchanger CalX. *Neuron* **45**, 367–378.

[12] Gerster, U., 1997. A quantitative estimate of flash-induced Ca2+- and Na^+-influx and Na^+/Ca^{2+}-exchange in blowfly *Calliphora* photoreceptors. *Vis. Res.* **37**, 2477–2485.

[13] Chu, B., Postma, M. & Hardie, R. C., 2013. Fractional Ca^{2+} currents through TRP and TRPL channels in *Drosophila* photoreceptors. *Biophysical Journal* **104**, 1905–1916.

[14] Vallet, A. M., Coles, J. A., Eilbeck, J. C. & Scott, A. C., 1992. Membrane conductances involved in amplification of small signals by sodium channels in photoreceptors of drone honey bee. *J. Physiol.* **456**, 303–324.

[15] Laughlin, S. B., de Ruyter van Steveninck, R. R. & Anderson, J. C., 1998. The metabolic cost of neural information. *Nat. Neurosci.* **1**, 36–41.

[16] Weckström, M., Kouvalainen, E. & Juusola, M., 1992. Measurement of cell impedance in frequency domain using discontinuous current clamp and white-noise-modulated current injection. *Pflüg. Arch* **421**, 469–472.

[17] Bendat, J. S. & Piersol, A. G., 2011. *Random Data: Analysis and Measurement Procedures.* John Wiley & Sons.

[18] Kennelly, A. E., 1893. Impedance. *Transactions of the American Institute of Electrical Engineers* pp. 172–232.

[19] Eggleston, D. L., 2011. *Basic Electronics for Scientists and Engineers.* Cambridge, UK: Cambridge University Press, 1st edition.

[20] French, A. S., 1980. The linear dynamic properties of phototransduction in the fly compound eye. *J. Physiol.* **308**, 385–401.

[21] Juusola, M., Kouvalainen, E., Järvilehto, M. & Weckström, M., 1994. Contrast gain, signal-to-noise ratio, and linearity in light-adapted blowfly photoreceptors. *J. Gen. Physiol* **104**, 593–621.

[22] Mauro, A., Conti, F., Dodge, F. & Schor, R., 1970. Subthreshold behavior and phenomenological impedance of the squid giant axon. *J. Gen. Physiol.* **55**, 497–523.

[23] DeFelice, L. J., 1981. *Introduction to membrane noise.* Plenum Press.

[24] Koch, C., 1984. Cable theory in neurons with active, linearized membranes. *Biol. Cybern.* **50**, 15–33.

[25] Hutcheon, B., Miura, R. M. & Puil, E., 1996. Models of subthreshold membrane resonance in neocortical neurons. *J. Neurophysiol.* **76**, 698–714.

[26] Davis, A. M., 1998. *Linear Circuit Analysis.* Boston: PWS Publishing Company.

[27] Bechhoefer, J., 2005. Feedback for physicists: A tutorial essay on control. *Rev. Mod. Phys.* **77**, 783–836.

[28] Anderson, J., 2000. *Membrane design and the performance of fly photoreceptors*. Cambridge, UK: University of Cambridge.

[29] Hamilton, W. R., 1841. Researches respecting vibration, connected with the theory of light. *Proc. Roy. Irish Acad.* **1**, 341–349.

[30] Brillouin, L., 1960. *Wave Propagation and Group Velocity*. Academic Press.

[31] Mohan, S., Hershenson, M., Boyd, S. & Lee, T., 2000. Bandwidth extension in CMOS with optimized on-chip inductors. *IEEE J. Solid-St. Circ.* **35**, 346–355.

[32] Frolov, R. V., 2016. Current advances in invertebrate vision: insights from patch-clamp studies of photoreceptors in apposition eyes. *J. Neurophysiol.* **116**, 709–723.

[33] van Hateren, J. H., 1986. An efficient algorithm for cable theory, applied to blowfly photoreceptor cells and LMC's. *Biol. Cybern.* **54**, 301–311.

[34] van Hateren, J. H., 1986. Electrical coupling of neuro-ommatidial photoreceptor cells in the blowfly. *J. Comp. Physiol. A* **158**, 795–811.